Investigation and Modeling of Ice Clouds Affecting Earth-space Communication Systems

Lorenzo Luini, *Senior Member, IEEE*, Andrea Quadri

***Abstract*— A model for ice clouds oriented to providing a useful tool for the accurate assessment of the impact of ice particles on Earth-space communications systems is presented. The model, developed starting from the data collected by the CloudSat LEO satellite, allows to synthesize vertical profiles of the ice water content from the sole knowledge of the whole integrated ice water content, which, in turn, can be typically obtained from Numerical Weather Prediction models or as a remote sensing product of Earth observation satellites. Moreover, the base of ice clouds is investigated and modeled, separately for mid- and high-altitude clouds, mostly consisting only of ice particles, and for low-level clouds, typically composed by both ice and liquid water. In addition, the impact of ice clouds on Earth-space optical links is preliminary investigated. Results, obtained for two sites, indicate that the attenuation due to ice is not negligible at optical wavelengths, as it can be in the order of tens of dBs on zenithal paths. The present model is intended to be integrated into a broader simulator of weather disturbances affecting electromagnetic wave propagation, conceived to support the design and performance assessment of Earth-space Communication Systems (EHF range or optical wavelengths).**

***Index Terms*— Electromagnetic propagation, ice cloud effects, satellite communications.**

I. Introduction

The request for advanced services (e.g. Internet connectivity via satellite), which are becoming progressively more and more complex, has been gradually pushing satellite communication (SatCom) systems to employ frequencies higher than the traditional (and congested) Ku band. Nowadays, the most advanced commercial systems, such as the Ka-SAT satellite by Eutelsat [1] in geostationary orbit (GEO), and the O3b fleet in Medium Earth Orbit (MEO) [2], operate at frequencies roughly up to 30 GHz, but in the near future also the Q and V bands will be addressed to increase the system capacity and the data rates offered to users. Even the W band [3] and optical wavelengths [4] have been recently considered as possible options for future SatCom systems. Besides increasing the operational frequency, the system capacity can also be boosted by implementing dual polarization, which allows, in principle, to double the link throughput using the same amount of bandwidth [5].

As is well known, the atmosphere produces strong detrimental effects on electromagnetic (EM) waves, especially at frequencies higher than 10 GHz; in fact the wavelength becomes comparable to the size of hydrometeors, which cause absorption and scattering of the radiated electromagnetic power. Besides rain attenuation, which plays the prevalent role for centimeter- and millimeter-wave communications [6], also other effects must be taken into account for the accurate design of Earth-space links, especially if frequencies beyond the Ka band are considered: for instance, the absorption caused by gases [7],[8], and the attenuation induced by clouds [9],[10]. While the latter effect is specifically associated to the impact of suspended droplets forming liquid water clouds, the presence of ice clouds along the link is often not considered because of the very low attenuation induced by ice particles [11]. Nevertheless, the impact of ice clouds on Earth-space communications is far from being negligible: on the one hand, they induce high levels of attenuation at optical wavelengths [12], and, on the other hand, they cause wave depolarization due to the marked anisotropy of ice particles (e.g. needles and plates) [13].

In order to increase the understanding of the impact of ice clouds on EM waves (as well as to predict it) in scenarios involving systems more complex than the typical single Earth-GEO satellite link (e.g. links to MEO and Low Earth Orbit – LEO – satellites or diversity schemes consisting of multiple ground stations), the most accurate approach is to simulate the microphysical interaction between ice particles and the wave front. In turn, this calls for the availability of ice cloud data at fine spatial resolution and with high accuracy, which, unfortunately, can be hardly obtained on global basis. As a result, accurate and reliable models aiming at synthesizing realistic vertical profiles of the ice water content are important. The only model of this kind available in the literature, to the authors' knowledge, is presented in [14], in which the Salonen-Uppala cloud identification model [10], originally devised only for liquid water clouds, is extended to provide also the prediction of the ice water content along the profile. Though of great usefulness, the model in [14] requires as input full vertical profiles of pressure, temperature and relative humidity, which are typically collected only two or four times per day, and only at specific sites (e.g. airports).

This contribution presents the investigation and modeling of ice clouds to allow the accurate assessment of their impact on

Manuscript received XXXX.

Lorenzo Luini is with the Dipartimento di Elettronica, Informazione e Bioingegneria, Politecnico di Milano, Piazza Leonardo da Vinci 32, 20133, Milano, Italy, and with the Istituto di Elettronica e di Ingegneria dell'Informazione e delle Telecomunicazioni (IEIIT), Consiglio Nazionale delle Ricerche, Via Ponzio 34/5, Milano 20133, Italy (e-mail: lorenzo.luini@polimi.it).

Andrea Quadri is with SIAE Microelettronica, Milan, Italy (e-mail: andrea.quadri@hotmail.it).

Earth-space communications systems. In fact, the final goal is to integrate the model developed in this paper into SMOC (Stochastic Model Of Clouds), presented in [18], in order to extend its applicability to the synthesis of full high-resolution three-dimensional (3-D) cloud fields, i.e. including both ice and liquid water. Eventually, both models will represent a significant part of a broader simulator of weather disturbances affecting electromagnetic wave propagation, conceived to support the design and performance assessment of Earth-space Communication Systems (EHF range or optical wavelengths) [19].

The remainder of this paper is organized as follows: the data collected by the CloudSat Earth Observation satellite, on the basis of which the model is developed, are described in detail in Section II. Section III deals with the analysis of the reference data to derive information on the profile of the ice water content in clouds, $i(h)$, which is afterwards exploited to derive a simple analytical expression for $i(h)$, whose parameters depend only on the integrated ice water content I; the last part of the section also addresses the modeling of the cloud base height h_0. Section IV deals with an example of the possible applications for the model developed in this contribution by addressing the fade induced by ice clouds on Earth-space Free Space Optical (FSO) links. Finally Section V draws some conclusions and outlines future work.

II. The Ice Cloud Dataset

CloudSat is an Earth observation satellite launched in 2006 by NASA to monitor clouds from space on global basis. The satellite, which is part of the large A-Train LEO (Low Earth Orbit) constellation (additionally composed by the Aqua, CALIPSO, PARASOL and Aura satellites), embarks a 94-GHz nadir-looking radar (Cloud Profiling Radar, CPR), which is used to estimate the vertical profile of the water content in clouds by receiving the electromagnetic power backscatter by liquid droplets and ice particles. Measurements are collected with high spatial resolution (the footprint is 1.4 km×1.7 km and the vertical profile is sampled every 240 m), between the ground and 25 km of altitude [15].

In order to study the main features of ice clouds, we have downloaded and processed the 2B-CWC-RVOD product (full 2009 year) assembled and made available by the Cooperative Institute for Research in the Atmosphere (CIRA) at the Colorado State University [16], which includes the most accurate estimate of the cloud ice water content i and of the liquid water content w: in fact, besides standard calibration and quality checks common to all 2B Level Products, cloud data are obtained by merging measurements collected by the CPR (reflectivity) and by the MODIS sensor (visible optical depth), that is part of the A-Train constellation as well [16]. More specifically, the methodology performs separate ice and liquid water retrievals using CloudSat and MODIS data. Both of these retrievals first assume that the radar profile is due to a single phase of water, that is, that the entire profile consists of either liquid water or ice; afterwards, the resulting separate profiles are combined using a simple scheme based on temperature as reported by an ECMWF model. The retrieval of w and i relies on the algorithms proposed in [20] and in [21], both of which assume lognormal distribution for the size of cloud droplets and for ice crystals and aim at retrieving w/i and the effective radius r_e, which can be analytically related to the main parameters defining univocally the lognormal distribution, including the particle number density N_T. The inversion of the combined CoudSat and MODIS data is achieved by implementing the retrieval approach proposed by Rogers [22], which provides a measure of the uncertainty in the retrieval, i.e. an indication of the data accuracy. This information is used by CIRA to mark and exclude unreliable profiles.

Fig. 1 shows a typical LEO orbit travelled by the CloudSat satellite (top) and sample vertical profiles of w (blue solid line) and i (dashed red line) expressed in g/m^3 (bottom), for a specific position of the CloudSat satellite along the orbit: in this case, the CPR identifies a low altitude cloud (≈ 1 km) composed only by liquid particles and an ice only cloud around 9 km from the ground.

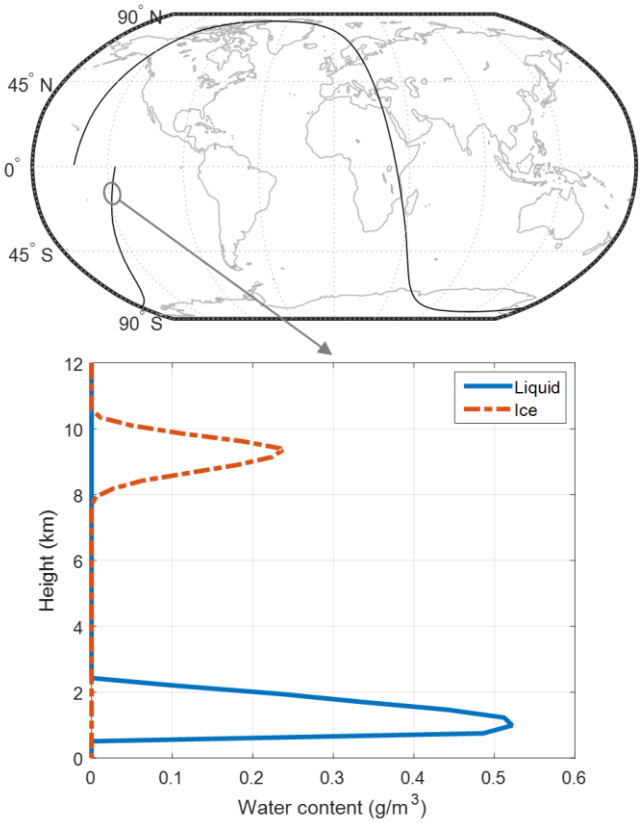

Fig. 1. Typical orbit travelled by the CloudSat satellite (top) and sample vertical profiles of w (blue solid line) and i (red dashed line) expressed in g/m^3 (bottom).

III. Ice Cloud Profile Model

A. Ice Water Content Profile

More than 880000 ice clouds were identified by processing the large CloudSat dataset mentioned in Section II. The preliminary visual inspection of CloudSat-derived profiles

This article has been accepted for publication in a future issue of this journal, but has not been fully edited. Content may change prior to final publication. Citation information: DOI 10.1109/TAP.2017.2772839, IEEE Transactions on Antennas and Propagation

highlighted that the vertical distribution of the reference ice water content $i(h)$ tends to be symmetric around its peak. This is evident in Fig. 1, as well as in Fig. 2, showing two additional profiles extracted from CloudSat data: the left graph depicts a large heavy ice clouds (the integrated ice water content I is 0.99 mm), while the one on the right reports a thinner and much less dense cloud (I = 0.04 mm).

Based on the observation of several profiles, the following analytical formulation was found to be a good choice to model $i(h)$ (h km a.m.s.l.):

$$i_S(h) = \begin{cases} \dfrac{I}{\sigma\sqrt{2\pi}} e^{-\frac{[(h-h_0)-\mu]^2}{2\sigma^2}} & \text{for } h \geq h_0 \\ 0 & \text{for } h < h_0 \end{cases} \quad (1)$$

In (1), h_0 is the cloud base height (discussed in detail later on in Section III.C), while μ and σ are parameters shaping the synthetic cloud profile, specifically by changing the position of its peak and by modifying its thickness, respectively.

It is easy to recognize the Gaussian distribution in the analytical expression in (1), which, however, is normalized to the cloud integrated ice water content I: in this way, the synthetic profile can be easily constrained to a given I value, provided that the expression in (1) is truncated to model real clouds, such that $i_S(h)$ is set to 0 for $i_S(h) < i_{th}$. Other analytical profiles were considered (e.g. Logistic distribution), but the Gaussian expression in (1) turned out to be the one reproducing at best the CloudSat-derived i profile.

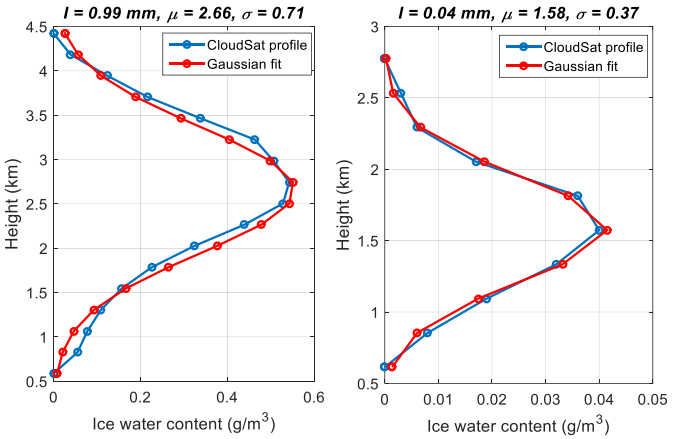

Fig. 2. Sample vertical profiles of the reference ice water content $i(h)$ as measured by the CPR on-board the CloudSat satellite and as estimated using the expression in (1).

For each cloud profile, first μ and σ in (1) were determined starting from $i(h)$ values and using Maximum Likelihood Estimation (MLE). Afterwards, the optimum value for i_{th} = 0.0225I was selected by seeking the overall best compromise between matching at best the thickness of real ice clouds (the lower is i_{th}, the larger, and less realistic, will be the synthetic cloud base) and by limiting the inevitable underestimation of the integrated ice water content caused by the truncation of the profile (the error obviously increases as also i_{th} increases). In order to quantify both aspects, we have defined, and minimized, the following error figures:

$$\varepsilon_T = 100\frac{T_S - T_R}{T_R} \quad \text{and} \quad \varepsilon_I = 100\frac{I_S - I_R}{I_R} \quad (2)$$

ε_T and ε_I are associated to the cloud thickness T and to the integrate ice water content I, respectively, while subscripts S and R refer to the synthetic profile in (1) and to the data collected by the CloudSat CPR, respectively.

Fig. 3 depicts the histogram of ε_T derived from all ice cloud profiles, which indicates that the cloud thickness is reproduced with satisfactory accuracy, i.e. for ε_T mainly ranging between -20% and 20%. This is confirmed by the average and root mean square error of ε_T, equal to E_T = 0.4% and RMS_T = 10.3%, respectively. Even lower values are found for ε_I, as depicted in the histogram of Fig. 4: for almost all ice clouds, the underestimation of I due to the truncation of the analytical profile in (1) is limited to -8%, being the average and root mean square value of ε_I equal to E_I = -1.5% and RMS_I = 1.9%, respectively.

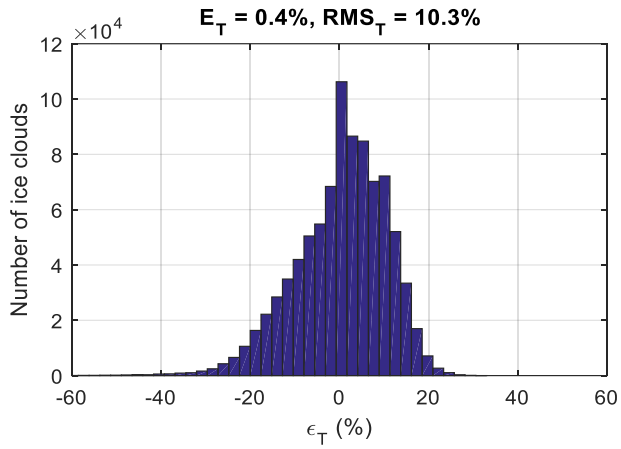

Fig. 3. Histogram of ε_T in (2); the title reports its average (E_T) and root mean square (RMS_T) values.

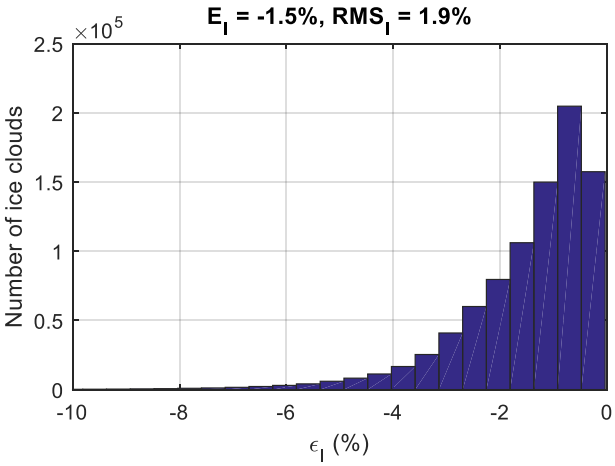

Fig. 4. Histogram of ε_I in (2); the title reports its average (E_I) and root mean square (RMS_I) values.

This article has been accepted for publication in a future issue of this journal, but has not been fully edited. Content may change prior to final publication. Citation information: DOI 10.1109/TAP.2017.2772839, IEEE Transactions on Antennas and Propagation

Another key indicator of how accurately the Gaussian profile in (1) can model ice clouds is provided by the error on the ice water content *i*:

$$\varepsilon_i(h) = i_S(h) - i_R(h) \tag{3}$$

As for (2), *S* and *R* are relative to the synthetic and CPR-derived profiles, but in this case, we employ an absolute error figure (expressed in g/m^3) rather than a percentage one, in order to avoid extreme values of $\varepsilon_i(h)$ biased by $i_R(h)$ samples approaching zero (the lowest value of $i_R(h)$ found in CloudSat data is 0.001 g/m^3).

Fig. 5 reports the statistical distribution of RMS$_i$, calculated, for each ice cloud, as the root mean square value of $\varepsilon_i(h)$: for almost all profiles, RMS$_i$ is limited to 0.04 g/m^3, it is prevalently lower than 0.004 g/m^3 (first two bars of the histogram) and its average value $\overline{RMS_i}$ is 0.0078 g/m^3. Overall, these results point out a good accuracy of the Gaussian profile in (1) in modeling ice clouds, considering, as a reference, that the average value of $i_R(h)$ in the database is $\overline{i_R(h)}$ = 0.059 g/m^3 (100 $\overline{RMS_i}$ / $\overline{i_R(h)}$ ≈ 13%).

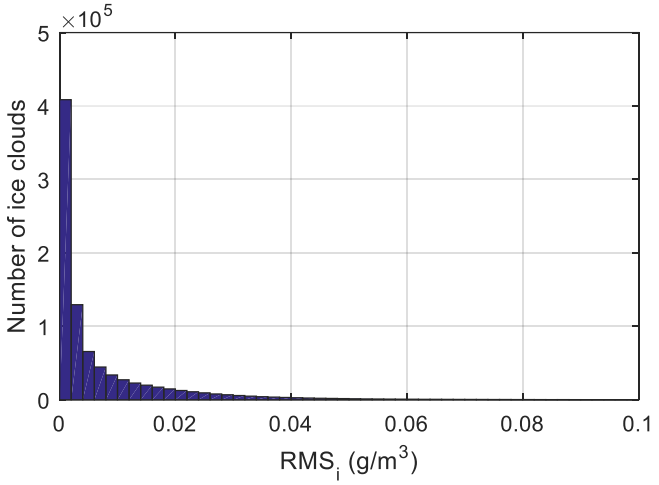

Fig. 5. Histogram of *RMS*$_i$.

B. Profile Parameters

The next step in modeling ice clouds consists in investigating μ and σ, with the specific goal of identifying analytical relationships between such parameters and the integrated ice water content *I*, which can be typically obtained from Numerical Weather Prediction models [17] or as a remote sensing product of Earth observation satellites.

Fig. 6 reports the density scatter plot (darker areas indicate a higher concentration of samples) between μ in (1) and *I*, obtained from the whole CloudSat dataset. Specifically, for each cloud, μ was derived from *i*(*h*) values after shifting the whole profile down to ground level: in this way, μ provides information only on the cloud shape (i.e. on how distant the peak ice water content is from the cloud base) and not on h_0, which is modelled separately later on in Section III.C.

As is clear from Fig. 6, the following analytical expression can represent with good accuracy the relationship between μ and *I* (red solid line):

$$\mu = 3.567\, I^{0.063} - 1.82\, e^{-3.635 I} - 0.284 \tag{4}$$

Also the relationship between σ and *I* was investigated, but the associated scatterplot was found to be much more dispersed than the one in Fig. 6. On the other hand, as depicted in Fig. 7, σ turns out to be linearly correlated to μ, such that the farther is the peak ice water content from the cloud base, the larger tends to be the cloud. Specifically, the relationship between μ and σ is well fitted by the following formula (red solid line in Fig. 7).

$$\sigma = 0.419\,\mu - 0.033 \tag{5}$$

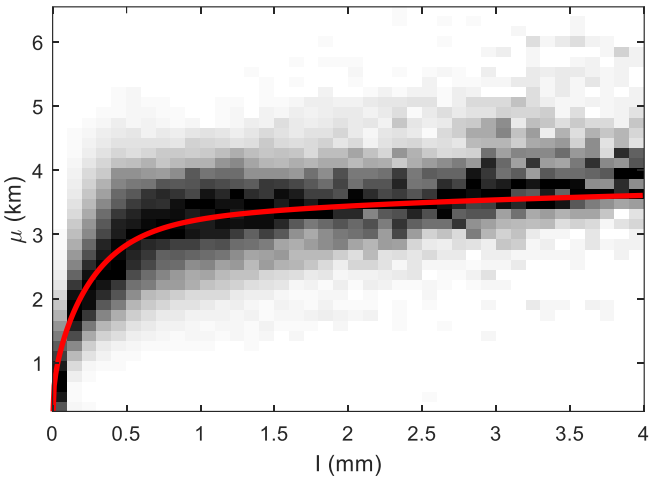

Fig. 6. Relationship between μ in (1) and *I*: density scatter plot (gray scale, higher concentration of samples in darker areas) based on CloudSat data and regression curve (red solid line).

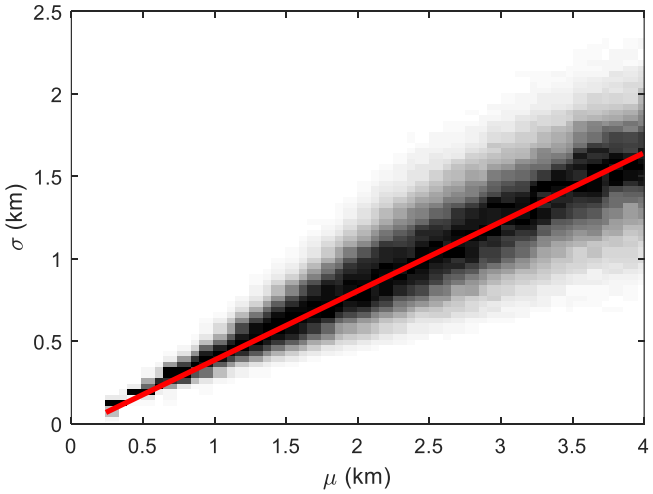

Fig. 7. Relationship between σ and μ in (1): density scatter plot (gray scale, higher concentration of samples in darker areas) based on CloudSat data and regression curve (red solid line).

As a result, exploiting (1), (4) and (5), for any given value of the cloud integrated ice water content I, a realistic ice cloud can be derived: Fig. 8 shows some sample profiles obtained using different input values for I, and all having the same reference cloud base, h_0 = 2 km. As, expected, the larger is I, the wider and denser will be the ice cloud.

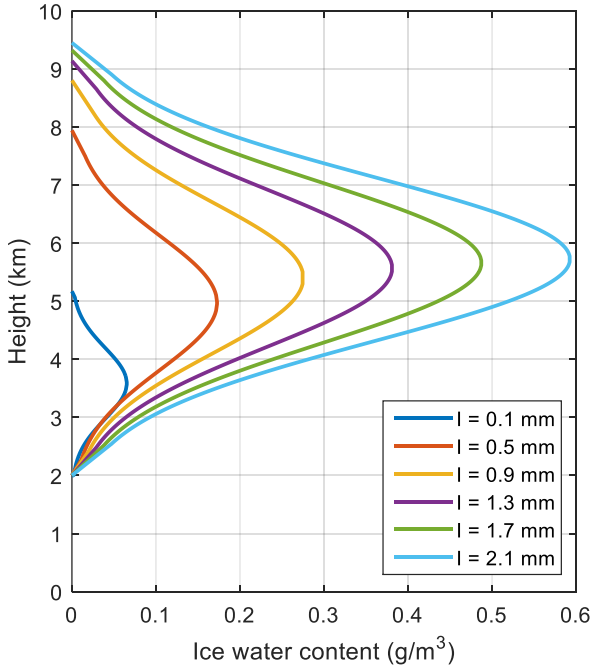

Fig. 8. Synthetic ice cloud profiles derived using (1), (4) and (5).

C. Ice Cloud Base

The whole CloudSat dataset was processed to extract information on the ice cloud base height h_0, which is key to complete the model presented in this contribution and might have a significant impact in investigating the effects of clouds on communication systems for aeronautical applications (e.g. Unmanned Aerial Vehicles, high-altitude drones, airliners, etc.). It is worth pointing out that the CPR, as any radar system, is likely to show intrinsic limitations in detecting small ice crystals/liquid water droplets, which, in turn, might decrease the accuracy of the retrieved h_0.

As a first step, the dataset was thoroughly investigated to identify some possible relationship between h_0 and other features of the cloud (e.g. thickness, integrated ice water content, maximum value of $i(h)$ along the profile, …) but no clear correlation was found. Therefore, we resorted to a simpler approach focusing on studying h_0 separately for different cloud types. More in detail, as a preliminary step, we have classified ice clouds on the basis of the whole CPR-derived profile, i.e. by considering also the presence of liquid water. Being N_T = 881892 the total number of ice clouds extracted from the CloudSat dataset, ice-only clouds were identified in approximately 30% of the cases, while CPR-derived profiles were found to be composed both by ice and liquid water (refer to Fig. 9 for a sample CPR-derived profile including both ice and liquid water clouds) in the remaining cases.

Fig. 10 shows the probability density function (PDF) of h_0 for ice-only clouds: besides showing that h_0 in this case can be accurately modeled by a Gaussian distribution (μ = 7.01, σ = 2.42), the figure also points out that, where no liquid water clouds are present, ice clouds lie on average, around 7 km from the ground, which is typically the case for mid- and high-altitude clouds.

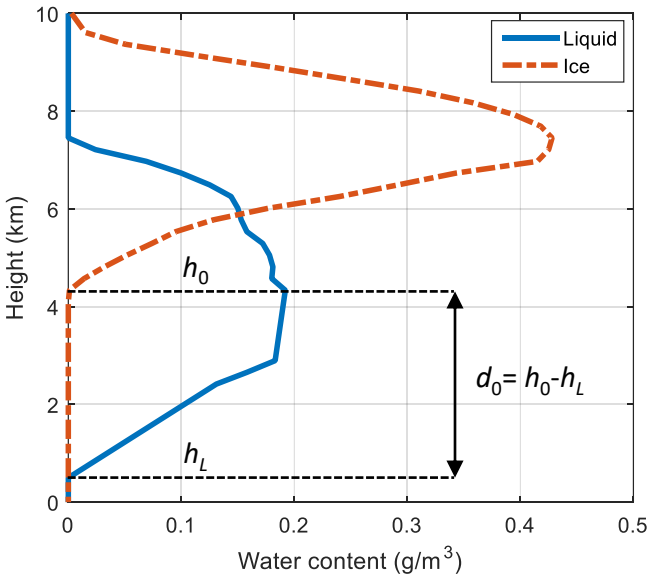

Fig. 9. Sample CPR-derived profile composed by both ice and liquid water; also shown is the distance d_0 between the ice cloud base and the liquid water cloud base.

As for clouds composed both by ice and liquid water (typically, low-level clouds), especially in the light of working towards the development of a model aimed at synthesizing full cloud fields [18], rather then studying h_0, it is worth investigating the statistics of d_0, defined as the distance between the ice cloud base h_0 and the liquid water cloud h_L (see Fig. 9): in fact, the knowledge of d_0 allows to preserve the spatial (vertical) correlation between ice and liquid water clouds. Fig. 11 shows the PDF of d_0 as obtained from CloudSat data, together with the MLE generalized extreme value distribution fitting the data (shape parameter ξ = 2.55, scale parameter σ = 0.5 and location parameter μ = 0.255), whose PDF has the following expression:

$$f(d_0)=\frac{1}{\sigma}t(d_0)^{\xi+1}e^{-t(d_0)} \quad \text{with} \quad t(d_0)=\left[1+\xi\left(\frac{d_0-\mu}{\sigma}\right)\right]^{-\frac{1}{\xi}} \tag{6}$$

As it is clear from the PDF, the distance between the two clouds is mostly quite limited, though it can amount to a few kilometers in some rare cases.

This article has been accepted for publication in a future issue of this journal, but has not been fully edited. Content may change prior to final publication. Citation information: DOI 10.1109/TAP.2017.2772839, IEEE Transactions on Antennas and Propagation

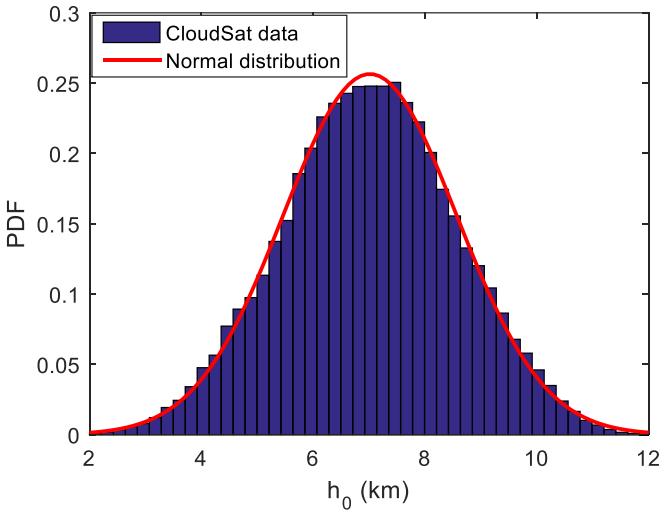

Fig. 10. Probability density function of h_0 for CPR-derived profiles consisting only of ice clouds; also shown is the fitting MLE Gaussian distribution ($\mu = 7.01$, $\sigma = 2.42$).

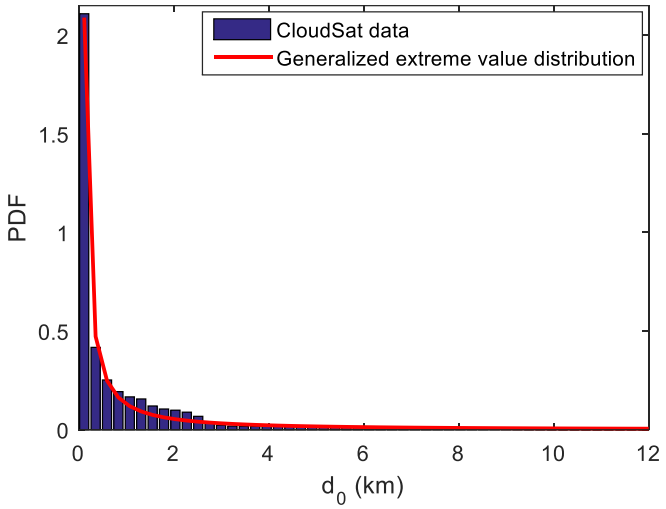

Fig. 11. Probability density function of d_0 for CPR-derived profiles consisting both of ice and liquid water; also shown is the fitting MLE generalized extreme value distribution (shape parameter $\xi = 2.55$, scale parameter $\sigma = 0.5$ and location parameter $\mu = 0.255$).

IV. Impact of Ice Clouds on Earth-space Optical Links

As an example of the possible applications for the model developed in this contribution, this Section deals with the fade induced by ice clouds on Earth-space Free Space Optical (FSO) links. Indeed, as briefly mentioned in Section I, some works have recently investigated the performance of SatCom systems featuring FSO feeder links [4],[23],[24],[25] though focusing only on the fade induced by liquid water clouds, A_L: the extinction properties of liquid water droplets at optical wavelengths are in fact so high that even very light clouds are sufficient to cause total blockage of the beam [26]; as a result, in most of the works mentioned above, ice cloud attenuation A_I is in fact neglected [23],[27], or taken into account using fixed reference values (e.g. in [4], the maximum A_i is assumed to be 5.4 dB).

The model proposed in this contribution offers the chance to better investigate the effects of ice clouds on FSO links. To this aim, we have extracted from ECMWF (European Centre for Medium-range Weather forecast) values of integrated ice water content I (three full years, from 2014 to 2016), provided every 6 hours on a regular latitude×longitude grid with 0.125°×0.125° spatial resolution (roughly corresponding to 10 km×10 km at mid-latitudes) [17]. Afterwards, for each value of I, the vertical profile of the ice water content $i(h)$ was derived by combining the model's equation, specifically (1), (4) and (5). This is a necessary step to estimate the specific attenuation induced by ice particles γ_I, which, according to [12], can be calculated as:

$$\gamma_I(h) = 40.26\, i(h)^{0.68} \tag{7}$$

where γ_I and $i(h)$ are expressed in dB/km and g/m^3, respectively. Equation (6) was derived by Platt, who investigated the particle size distribution (PSD) of ice particles of different shape and with dimension ranging between 2 μm and 3 mm. Specifically, Platt first proposed equations modeling i and y_I as a function of the PSD and for some different particle shapes. Equation (6) was then obtained as the overall best power-law fitting the numerical calculations relying on such equations and on the collected PSD data, for three specific particle shapes: bullets, columns and plates. Note that equation (6) does not depend on the wavelength, as it was derived under the assumption that ice particles are large compared to wavelengths in the optical range (optical limit approximation): in this case, the scattering cross section can be simply calculated as two times the geometrical section of the particle [12]. Other expressions for the calculation of the specific attenuation due to ice are available in the literature: as an example, it is worth citing the work in [28], where the authors show that γ_I is function both of i and of the ice particle concentration N_i. A more comprehensive analysis of the methodologies to predict the effects induced by ice on FSO links will be the subject of following contributions: in fact, this Section is more intended just as an example showing the applicability of the proposed ice cloud model to propagation-oriented applications.

As a final step, the path attenuation due to ice A_I is calculated by integrating γ_I along the path (Z is the portion of the link crossing the ice cloud):

$$A_I = \int_Z \gamma_I(h)\, dh \tag{8}$$

The integration in (7) is performed numerically and considering a zenithal path: though this is not a realistic case for typical Earth-space links, this exercise provides a preliminary indication of the path attenuation due to ice clouds to be expected on FSO links. In fact, more complex simulations involving slant paths require taking into account also the horizontal variability of clouds [29], which will be

This article has been accepted for publication in a future issue of this journal, but has not been fully edited. Content may change prior to final publication. Citation information: DOI 10.1109/TAP.2017.2772839, IEEE Transactions on Antennas and Propagation

subject of investigation in following contributions. Finally, it is worth mentioning that, in this simple application, the choice of the cloud base has no effect on the values of A_I derived through (7), and therefore we have set h_0 = 2 km for all the $i(h)$ profiles.

Fig. 12 depicts the mean yearly Complementary Cumulative Distribution Function (CCDF) of A_I as derived from the whole ECMWF dataset for two reference sites: Spino d'Adda (45.4° N, 9.5° E), in Northern Italy, close to Milan, and Tito Scalo (40.6° N, 15.7° E) in Southern Italy, close to Potenza. Fig. 12 reports the results derived from taking into account only the effect induced by ice, but considering all ice clouds, i.e. regardless of the presence of l along the profile (any cloud containing some i was included in the calculation). Results indicate that ice clouds induce a significant attenuation on FSO links (as a reference, the wavelength is set to λ = 1.55 μm), which is expected to increase even more for slant paths. In fact, the probability for the link to be affected by ice clouds in a year is 53% and 65%, for a ground station in Tito Scalo and Spino d'Adda, respectively, and approximately 20 dB and 30 dB are exceeded for 1% of the yearly time in the two sites.

Fig. 13 reports the same information as in Fig. 12, but considering only ice clouds for which the integrated liquid water content L extracted from ECMWF is zero. This is typically the case of mid- and high-altitude ice clouds, which are generally less heavy than low-level ones. This is reflected by the lower value of A_I reported in Fig. 13: the probability for the link to be affected by clouds consisting only of ice particles is approximately 6% for both sites, and the attenuation exceeded for 1% of the time in a year reduces to roughly 3 dB and 5 dB for Spino d'Adda and Tito Scalo, respectively. Notwithstanding this, the highest values of A_I in this case, for both sites, range between 15 and 20 dB.

Overall, besides clearly showing that the effect of ice clouds on FSO links cannot be neglected, these preliminary results also highlight how the amount of A_I might differ from site to site, which, in turn, points out the importance of relying on accurate and flexible models to estimate the effects of clouds on Earth-space FSO links.

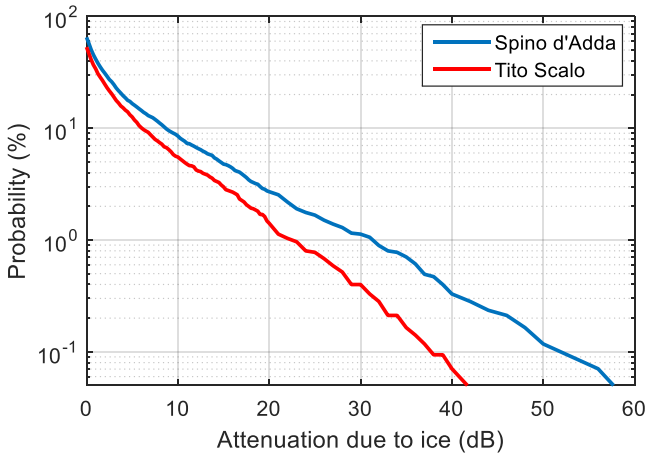

Fig. 12. Mean yearly CCDF of A_I as derived from the whole ECMWF dataset for Spino d'Adda and Tito Scalo.

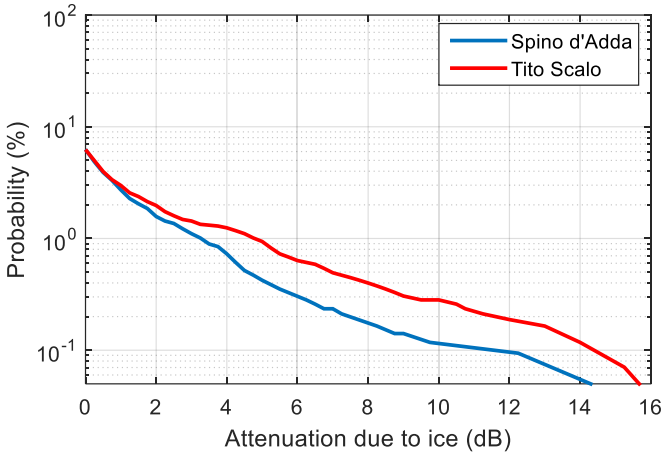

Fig. 13. Mean yearly CCDF of A_I as derived from the ECMWF dataset for Spino d'Adda and Tito Scalo, considering only ice clouds not associated to liquid water clouds.

V. Conclusions

This contribution presents a model to synthesize high-resolution vertical profiles of the water content in ice clouds, $i(h)$. The model is derived from the investigation of a large set of ice cloud data collected by the CPR on-board the CloudSat satellite. The thorough analysis of such data pointed out that $i(h)$ follows a truncated Gaussian probability density function normalized to the total integrated ice water content in the cloud, I, on which the mean and standard deviation values depend. Also the cloud base h_0 was investigated: for mid- and high-altitude clouds, h_0 turns out to be normally distributed (μ = 7.01, σ = 2.42), while for low-level clouds, typically composed of both ice particles and liquid water droplets, the distance between the ice and liquid water clouds (d_0) was found to follow a generalized extreme value distribution.

As an example of the possible applications for the model developed in this contribution, the fade induced by ice clouds on Earth-space Free Space Optical (FSO) links was investigated taking advantage of I data (available every 6 hours with 0.125°×0.125° spatial resolution) extracted from ECMWF, for three years and two sites. Preliminary results indicate that, even for zenithal paths, ice clouds induce a significant attenuation A_I on a 1.55-μm FSO link (considering all types of clouds, approximately 20 dB and 30 dB are exceeded for 1% of the yearly time in Tito Scalo and Spino d'Adda, respectively; considering ice-only clouds, such margins reduce to 3 dB and 5 dB) and that the amount of A_I might strongly differ from site to site. This, in turn, calls for the use of accurate and flexible models to estimate the effects of clouds on Earth-space FSO links.

The proposed model is intended to be integrated into a broader simulator of weather disturbances affecting EM wave propagation, conceived to support the design and performance assessment of Earth-space Communication Systems (EHF range or optical wavelengths): indeed, modeling ice clouds will also allow to investigate the depolarization affecting EHF SatCom systems, which is induced by the marked anisotropy of ice particles (e.g. needles and plates).

ACKNOWLEDGMENT

The authors would also like to acknowledge the CloudSat mission scientists and associated NASA personnel for the production of the data used in this work.

REFERENCES

[1] H. Fenech, S. Amos, A. Tomatis, V. Soumpholphakdy, "High throughput satellite systems: An analytical approach," *IEEE Transactions on Aerospace and Electronic Systems*, vol. 51, no. 1, Page(s): 192 - 202, 2015.

[2] S. H. Blumenthal, "Medium Earth Orbit Ka Band Satellite Communications System," in Proceeding of the 2013 IEEE Military Communications Conference, Page(s): 273 – 277, San Diego, California, USA, 18-20 November 2013.

[3] S. De Fina, M. Ruggieri, A. V. Bosisio, "Exploitation of the W-band for high capacity satellite communications," *IEEE Transactions on Aerospace and Electronic Systems*, vol. 39, no. 1, Page(s): 82 – 93, 2003.

[4] S. Poulenard, M. Crosnier, A. Rissons, "Ground Segment Design for Broadband Geostationary Satellite With Optical Feeder Link," *J. Opt. Commun. Netw.*, vol. 7, no. 4, Page(s): 325 – 336, 2015.

[5] P. Henarejos, A. I. Pérez-Neira, "Dual Polarized Modulation and Reception for Next Generation Mobile Satellite Communications," *IEEE Transactions on Communications*, vol. 63, no. 10, Page(s): 3803 – 3812, October 2015.

[6] R. K. Crane, "Electromagnetic Wave Propagation Through Rain," Wiley, ISBN: 978-0-471-61376-3, 288 pages, April 1996.

[7] L. Luini, C. Riva, "Improving the Accuracy in Predicting Water Vapor Attenuation at Millimeter-wave for Earth-space Applications", *IEEE Transactions on Antennas and Propagation*, vol. 64, no. 6, Page(s): 2487 - 2493, June 2016.

[8] H. J. Liebe, G. A. Hufford, and M. G. Cotton, "Propagation modeling of moist air and suspended water/ice particles at frequencies below 1000 GHz," in Proc. AGARD 52nd Spec. Meeting EM Wave Propag. Panel, Palma De Maiorca, Spain, 1993, pp. 3.1–3.10.

[9] L. Luini, C. Capsoni, "Efficient Calculation of Cloud Attenuation for Earth-space Applications", *IEEE Antennas and Wireless Propagation Letters*, vol. 13, Page(s): 1136 – 1139, 2014.

[10] E. Salonen, S. Uppala, "New prediction method of cloud attenuation," *Electron. Lett.*, vol. 27, no. 12, pp. 1106–1108, Jun. 1991.

[11] G. Brussaard, P. A. Watson, "Atmospheric Modelling and Millimetre Wave Propagation," Springer Science & Business Media, 31 December 1994.

[12] C. M. R. Platt, "A parametrization of the visible extinction coefficient of ice clouds in terms of the ice water content", *J. Atmos. Sci.*, vol. 54,. pp. 2083-2098, 1997.

[13] A. Paraboni, A. Martellucci, C. Capsoni, C. Riva, "The physical basis of atmospheric depolarization in slant paths in the V band: theory, Italsat experiment and models", *IEEE Transactions on Antennas and Propagation*, vol. 59, no. 11, Page(s): 4301-4314, November 2011.

[14] A. Martellucci, J. P. V. Poiares Baptista, G. Blarzino, "New climatological databases for ice depolarisation on satellite radio links," COST 280 "Propagation Impairment Mitigation for MillimetreWave Radio Systems", PM3037, 1st Int. Workshop, Jul. 2002, Malvern, U.K.

[15] G. L. Stephens, D. G. Vane, R. J. Boain, G. G. Mace, K. Sassen, Z. Wang, A. J. Illingworth, E. J. O'Connor, W. B. Rossow, S. L. Durden, S. D. Miller, R. T. Austin, A. Benedetti, C. Mitrescu, the CloudSat Science Team, "The CloudSat mission and the A-TRAIN: A new dimension to space-based observations of clouds and precipitation," 2002, Bull. Am. Met. Soc., 83, 1771-1790.

[16] N. Wood, "Level 2B Radar-Visible Optical Depth Cloud Water Content (2B-CWC-RVOD) Process Description Document," CloudSat project, Version 5.1, 23 October 2008.

[17] www.ecmwf.int. Accessed April 2017.

[18] L. Luini, C. Capsoni, "Modeling High Resolution 3-D Cloud Fields for Earth-space Communication Systems," *IEEE Transactions on Antennas and Propagation*, vol. 62, no. 10, Page(s): 5190 - 5199, October 2014.

[19] L. Luini, "A Comprehensive Methodology to Assess Tropospheric Fade Affecting Earth-Space Communication Systems", IEEE Transactions on Antennas and Propagation, vol. 65, no. 9, Page(s): 3654 - 3663, July 2017.

[20] R. T. Austin, G. L. Stephens, "Retrieval of stratus cloud microphysical parameters using millimeter-wave radar and visible optical depth in preparation for CloudSat, 1. Algorithm formulation," *J. Geophys. Res.*, 106, 28,233–28,242, 2001.

[21] R. T. Austin, A. J. Heymsfield, G. L. Stephens, "Retrieval of ice cloud microphysical parameters using the CloudSat millimeter-wave radar and temperature," *J. Geophys. Res.*, 114, D00A23, 2009.

[22] C. D. Rodgers, "Inverse Methods for Atmospheric Sounding: Theory and Practice," World Scientific Publishing, Singapore, 2000.

[23] N. K. Lyras, C. I. Kourogiorgas, A. D. Panagopoulos, "Joint Statistics of Cloud Attenuation induced on Multiple Optical Satellite Links," 21st Ka and Broadband Communications, Navigation and Earth Observation Conference, Bologna (Italy), pp. 1-7, 12-14 October, 2015.

[24] R. Mata-Calvo, D. Giggenbach, A. Le Pera, J. Poliak, R. Barrios, S. Dimitrov, "Optical Feeder Links For Very High Throughput Satellites – System Perspectives," 21st Ka and Broadband Communications, Navigation and Earth Observation Conference, Bologna (Italy), pp. 1-7, 12-14 October, 2015.

[25] N. Lyras, C. Kourogiorgas, A. Panagopoulos, "Cloud Free Line of Sight Prediction Modeling for Optical Satellite Communication Networks," IEEE Communications Letters , vol. 21, no. 7, pp.1537-1540.

[26] L. Luini, R. Nebuloni, C. Capsoni, "Effectiveness of Multisite Diversity Schemes to Support Optical Systems in Scientific Missions", *Optical Engineering* 53 (2), 026104 (Feb 18, 2014).

[27] N. K. Lyras, C. I. Kourogiorgas and A. D. Panagopoulos, "Cloud Attenuation Statistics Prediction From Ka-Band to Optical Frequencies: Integrated Liquid Water Content Field Synthesizer," IEEE Transactions on Antennas and Propagation, vol. 65, no. 1, pp. 319-328, Jan. 2017.

[28] I. Gultepe, B. Zhou, J. Milbrandt, A. Bott, Y. Li, A. J. Heymsfield, B. Ferrier, R. Ware, M. Pavolonis, T. Kuhn, J. Gurka, P. Liu, J. Cermak, "*A review on ice fog measurements and modeling*," Atmospheric Research 151 (2015) 2–19.

[29] L. Luini, C. Capsoni, "Scaling Cloud Attenuation Statistics with Link Elevation in Earth-space Applications", *IEEE Transactions on Antennas and Propagation*, vol. 64, no. 3, Page(s): 1089 - 1095, March 2016.